Monthly Notices
of the
ROYAL ASTRONOMICAL SOCIETY

Mon. Not. R. Astron. Soc. **407,** 1376–1386 (2010) doi:10.1111/j.1365-2966.2010.16926.x

Photometric and clustering properties of hydrodynamical galaxies in a cosmological volume: results at $z = 0$

Sebastián E. Nuza,[1⋆] Klaus Dolag[1] and Alexandro Saro[2,3]

[1]*Max Planck Institute for Astrophysics, Karl-Schwarzchild Str. 1, D85748 Garching, Germany*
[2]*Dipartamento di Astronomià dell'Universita di Trieste, via Tiepolo 11, I-34131 Trieste, Italy*
[3]*INFN-National Institute for Nuclear Physics, Trieste, Italy*

Accepted 2010 April 27. Received 2010 April 26; in original form 2010 February 23

ABSTRACT

In this work, we present results for the photometric and clustering properties of galaxies that arise in a Λ cold dark matter hydrodynamical simulation of the local Universe. The present-day distribution of matter was constructed to match the observed large-scale pattern of the *IRAS* 1.2-Jy galaxy survey. Our simulation follows the formation and evolution of galaxies in a cosmological sphere with a volume of $\sim 130^3\, h^{-3}\,\mathrm{Mpc}^3$ including supernova feedback, galactic winds, photoheating due to a uniform meta-galactic background and chemical enrichment of the gas and stellar populations. However, we do not consider active galactic nuclei. In the simulation, a total of $\sim$20 000 galaxies are formed above the resolution limit, and around 60 haloes are more massive than $\sim 10^{14}\,\mathrm{M}_\odot$. Luminosities of the galaxies are calculated based on a stellar population synthesis model including the attenuation by dust, which is calculated from the cold gas left within the simulated galaxies. Environmental effects such as colour bimodality and differential clustering power of the hydrodynamical galaxies are qualitatively similar to observed trends. Nevertheless, the overcooling present in the simulations leads to too blue and overluminous brightest cluster galaxies (BCGs). To overcome this, we mimic the late-time suppression of star formation in massive haloes by ignoring recently formed stars with the aid of a simple post-processing recipe. In this way we find luminosity functions, both for field and for group/cluster galaxies, in better agreement with observations. Specifically, the BCGs then follow the observed luminosity–halo mass relation. However, in such a case, the colour bimodality is basically lost, pointing towards a more complex interplay of late suppression of star formation than what is given by the simple scheme adopted.

Key words: hydrodynamics – methods: numerical – galaxies: evolution – galaxies: formation – cosmology: theory.

1 INTRODUCTION

The observational study of galaxy populations has seen an outstanding progress in recent years. With the advent of large galaxy redshift surveys, such as the Sloan Digital Sky Survey (SDSS; York et al. 2000) and the Two-degree Field Galaxy Redshift Survey (Colless et al. 2001), it was possible to extend our knowledge of the local Universe to a new level of accuracy.

In particular, it has been possible to carry out a robust determination of the luminosity function (LF) for galaxies in the field (Norberg et al. 2002; Blanton et al. 2003) in different spectral bands and to better establish it for those galaxies populating denser environments, such as groups and clusters (e.g. Popesso et al. 2004, 2006). Consistently with previous work (e.g. Lin et al. 1996; Colless 1999) it has been found that the field LF is well described by a single Schechter function requiring, however, a higher value for the luminosity density of the Universe indicating that previous surveys suffered from selection effects and systematics due to photometry (Blanton et al. 2001). For higher density environments, and by means of the RASS-SDSS galaxy cluster survey, Popesso et al. (2004, 2006) found that a double Schechter function better fits the composite cluster LF accounting for a possible upturn in the number of faint objects as the luminosity of member galaxies decreases.

Moreover, the large number of galaxies with measured spectroscopic redshifts, compared to that obtained in the past, has made possible the determination of their two-point clustering properties in a reliable way out to scales of the order of tens of Mpc. These studies have shown that the real, projected and redshift–space correlations can be well described by a decreasing power-law function

⋆E-mail: sebasn@mpa-garching.mpg.de

that depends on the sample colour, having a correlation length that increases with absolute magnitude (e.g. Norberg et al. 2001, 2002; Zehavi et al. 2002; Hawkins et al. 2003; Madgwick et al. 2003).

Both the LFs and the clustering properties of the galaxies are tools of fundamental importance in the study of galaxy formation since they provide a way to describe the most basic galaxy statistics. A successful model for structure formation must account for these observations.

From the theoretical point of view, the widely spread *semi-analytic* models (SAMs) of galaxy formation (e.g. Kauffmann et al. 1999; Springel et al. 2001; Mathis et al. 2002; De Lucia, Kauffmann & White 2004, Springel et al. 2005; Bower et al. 2006; Cattaneo et al. 2006; Croton et al. 2006; Lagos, Cora & Padilla 2008; Fontanot et al. 2009; Guo & White 2009) provide a way to study the properties of galaxy populations with the advantage of a rapid exploration of the parameter space. In this approach, the galaxy population is followed within the skeleton provided by a parent dark matter simulation with the aid of physically motivated recipes to describe the different baryonic processes involved. These studies have pointed out the need for limiting excessive gas condensation in massive haloes to avoid the formation of very bright central galaxies [also known as brightest cluster galaxies (BCGs)] that are inconsistent with observation. The usually invoked channel responsible for the star formation (SF) quenching in massive haloes is the active galactic nucleus (AGN) phenomenon. Similarly, it has been noted that in order to prevent an excess luminosity in the faint end of the galaxy field LF, a relatively strong supernova (SN) feedback would be needed in smaller systems.

On the other hand, cosmological hydrodynamical simulations of galaxy samples, without including the effects of AGN feedback, have also been used to study the building up of the structure and their resulting properties in periodic boxes (e.g. Pearce et al. 2001; White, Hernquist & Springel 2001; Yoshikawa et al. 2001, Oppenheimer & Davé 2006, 2008; Davé & Oppenheimer 2007; Ocvirk, Pichon & Teyssier 2008). In a similar way, using the dubbed *zooming* technique, several authors simulated hydrodynamical galaxies within high-resolution regions in a cosmological framework (e.g. Dolag et al. 2005; Saro et al. 2006, 2008, 2009; Crain et al. 2009). In particular, Saro et al. (2006) resimulated a set of galaxy clusters studying the composite cluster LF and the environmental induced galaxy properties in these high density regions. These authors show that it is possible to reproduce the general observed trends of the cluster galaxy population, including e.g. the colour–magnitude relation, the age and colour cluster-centric distance dependence and the cluster LF (although the bright end is affected by the presence of very bright BCGs).

This work makes use of the same *zooming* technique to simulate the observed local volume following the chemical enrichment of gas and stars until the present epoch. This enables us to estimate in a consistent way the luminosities and colours of galaxies formed in hydrodynamical simulations. The simulated volume is big enough to compute LFs, both for field and for group/cluster galaxies, as well as galaxy correlation functions. In order to infer the way feedback acts in massive haloes (e.g. AGN feedback), we use a similar approach to SAMs, applying a simple recipe to the post-processed data of the simulation at $z = 0$. In this way, we ignore a fraction of the late-formed stars which would not appear in such a scenario and study the resulting effects on the luminosity-dependent properties of the simulated galaxies. It is important to note that, within the simple post-processing scheme adopted here, the simulations are no longer fully self-consistent, since also stars which are quenched by our post-processing procedure still interact with the surrounding medium. However, this effect is not expected to change our results significantly and can only be accessed with the next generation of hydrodynamical simulations including sub-scale models for AGN feedback more directly.

This paper is organized as follows. In Section 2 we describe the hydrodynamical cosmological simulation, together with the method used to compute galaxy luminosities and the associated dust obscuration. In Section 3 we show the main results, presenting luminosities (for field and group/cluster galaxies), galaxy colours and correlation functions. We also discuss the implemented recipe to *suppress* SF in massive haloes. Finally, we close the paper with a summary and our conclusions in Section 4.

2 THE SIMULATION

The cosmological simulation analysed in this paper was generated to reproduce the large-scale distribution of matter in the local Universe within the context of a flat ΛCDM scenario. The cosmological parameters at present time are a matter density parameter $\Omega_{\rm m} = 0.3$, a baryon density parameter $\Omega_{\rm b} = 0.04$, a Hubble constant $H_0 = 100\,h\,{\rm km\,s^{-1}\,Mpc^{-1}}$ with $h = 0.7$ and an rms density fluctuation $\sigma_8 = 0.9$, which correspond to the *Wilkinson Microwave Anisotropy Probe* 1-yr best-fitting cosmology (Spergel et al. 2003).

In order to reproduce the local matter density field, the galaxy distribution in the *IRAS* 1.2-Jy galaxy survey (Fisher et al. 1994, 1995) was Gaussianly smoothed on a scale of 7 Mpc and then linearly evolved back in time up to $z = 50$ with the method proposed by Kolatt et al. (1996). The resulting high-redshift field is then used as a Gaussian constraint (Hoffman & Ribak 1991) to assign the unperturbed positions of 2×51 million gas and dark matter particles that are arranged on a glass-like distribution (e.g. Baugh, Gaztañaga & Efstathiou 1995). The mass of gas and dark matter particles is set to 4.7×10^8 and $3.1 \times 10^9\,h^{-1}\,{\rm M}_\odot$, respectively. Every gas particle is able to produce three generations of stars, which result in a star particle mass of $\sim 1.6 \times 10^8\,h^{-1}\,{\rm M}_\odot$.

We follow the evolution of the collisionless and gas components within a sphere with a comoving diameter of $160\,h^{-1}$ Mpc that is embedded in a periodic cosmological box of $340\,h^{-1}$ Mpc on a side. This makes the volume of the simulated universe a factor of $\sim$2 times larger than in previous studies (e.g. Pearce et al. 2001). The region outside the sphere is sampled with approximately seven million low-resolution dark matter particles, which allow us to asses the effect of long-range gravitational tidal forces. The comoving softening length for gravitational forces is set to $7\,h^{-1}$ kpc (Plummer equivalent), a value that is similar to the average particle separation in the cores of the densest simulated clusters. In Fig. 1, we show the projected gas density distribution of the simulated local sphere.

The simulation was run using GADGET-2 (Springel & Hernquist 2002, 2003; Springel 2005) which is a tree-smoothed particle hydrodynamics code that fully conserves entropy during the evolution of the gas component, taking into account radiative cooling, heating by an ultraviolet (UV) meta-galactic background to emulate the reionization era (Haardt & Madau 1996) and a subresolution scheme to treat SF, SN feedback and galactic winds. In particular, the set of parameters of the phenomenological wind model was chosen to obtain an escape velocity of $480\,{\rm km\,s^{-1}}$. For the SF recipe we assume that each star particle of the simulation is a single stellar population (SSP) where the relative number of stars with different masses is obtained by means of the initial mass function, which in this work is that of Salpeter (1955) normalized in the 0.1–100 $\,{\rm M}_\odot$ mass range.

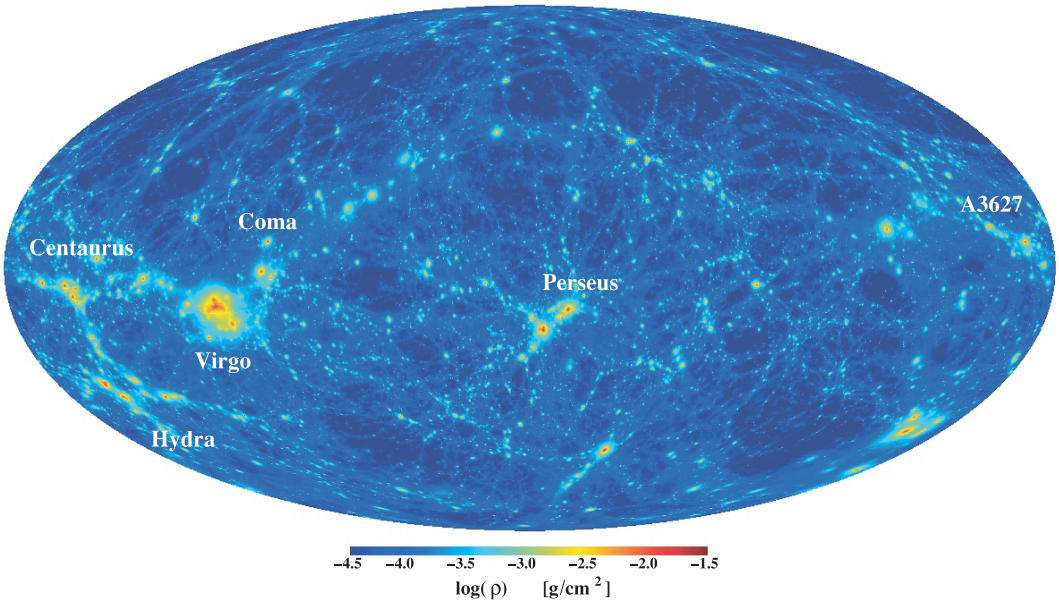

Figure 1. Full-sky map of the simulated local volume in supergalactic coordinates. The map displays the projected gas density distribution up to a distance of $\sim$80 Mpc h^{-1} from the observer where main galaxy clusters are shown. Note that Virgo cluster, being the closest one to the observer, is particularly prominent.

The metal content of gas and stellar components is followed using the model presented in Tornatore et al. (2004; see also Tornatore et al. 2007). This scheme accounts for stellar evolution assessing the effect of the generation of Type II and Type Ia SN events (SNII and SNIa, respectively), as well as of massive stars ending up their life in the asymptotic giant branch phase. These events release energy and metals to the surrounding medium according to the stellar lifetimes of the different populations (Maeder & Meynet 1989) and to the SNIa rate (Matteucci & Recchi 2001). It is assumed that energy feedback is only provided by SNs (10^{51} erg per event), while metals are distributed in all cases following the production of Fe, O, C, Si, Mg and S using the stellar yields found in Recchi, Matteucci & D'Ercole (2001). In addition, the local cooling rate for each gas particle is self-consistently determined from its estimated [Fe/H] abundance and temperature using the tables given by Sutherland & Dopita (1993). At each time-step, the network of primordial species is solved assuming that photoionization only acts on them. In this regard, we expect that metal photoionization will have only a minor impact at the resolution covered by our simulation.

Bound systems at the present time are identified using the SUBFIND algorithm (e.g. Springel et al. 2001; Dolag et al. 2009). First, haloes having more than 32 dark matter particles are selected using the friends-of-friends (FoF) algorithm with a linking length of 0.2 in units of the mean interparticle separation. Then, a total of 20, self-bound, particles (ignoring gas particles) are set as a lower limit to identify substructures present in each FoF group that may be eligible as galaxies. As the detection of substructures is difficult at the low-mass end, we consider as numerically *resolved* galaxies only substructures in the simulation having more than 32 star particles, which results in a stellar mass resolution limit of $\sim 7 \times 10^9\,\mathrm{M}_\odot$.

2.1 Luminosity of galaxies

2.1.1 Stellar population synthesis

Similar to Saro et al. (2006), we compute the luminosities of our simulated galaxies using the stellar population synthesis model of Bruzual & Charlot (2003) in different spectral bands. As mentioned in the previous section, each star particle is treated as an SSP with a formation time that corresponds to redshift z_i and metallicity content z_i. For every galaxy, this enables us to sum up the luminosity contributions L_i of each stellar population in the following way:

$$L(\lambda) = \sum_i L_i(\lambda, z_i, Z_i) \mathrm{e}^{-\tau_\lambda}, \tag{1}$$

where λ is the wavelength of radiation, $\mathrm{e}^{-\tau_\lambda}$ is the extinction factor due to the presence of dust (see e.g. Bruzual & Charlot 2003) and τ_λ is the wavelength-dependent optical depth of the obscuring medium (see the next section).

To compute the luminosities we use only stars inside the galactocentric distance that contain 83 per cent of the galaxy's baryonic mass, the so-called *optical radius* (e.g. Nuza et al. 2007). We have checked that adopting this condition has a negligible effect on the final absolute magnitudes.

2.1.2 Attenuation by dust

In order to asses the effect of dust in the luminosity of galaxies, we apply a similar procedure to Saro et al. (2009) to our hydrodynamical galaxies. The extinction model assumed is that of Charlot & Fall (2000). These authors considered a scenario where the radiation of newly born stars ($t \leq 10^7$ yr) is attenuated by the presence of dust in their birth cloud. Older stellar populations are able to migrate out of the molecular clouds and, as a consequence, are mainly affected by the ambient ISM. Therefore, we assume the following age-dependent extinction curve:

$$\frac{\tau_\lambda}{\tau_V} = \begin{cases} \left(\frac{\lambda}{550\ \mathrm{nm}}\right)^{-0.7} & t \leq 10^7\ \mathrm{yr} \\ \mu \left(\frac{\lambda}{550\ \mathrm{nm}}\right)^{-0.7} & t > 10^7\ \mathrm{yr} \end{cases}, \tag{2}$$

where τ_V is the optical depth in the V band, λ is the wavelength of radiation and μ is the fraction of the effective optical depth due to the ISM. In this paper, we take μ randomly from a Gaussian distribution centred in 0.3 with a width of 0.2 and truncated at 0.1

and 1 in the same way as done in previous works (e.g. De Lucia & Blaizot 2007).

Following Guiderdoni & Rocca-Volmerange (1987), we assume that τ_V is proportional to the column density of cold gas in the line of sight having mean metallicity Z_g. In particular, for the wavelengths of interest here, we can write

$$\tau_V = \left(\frac{Z_g}{Z_\odot}\right)^s \left(\frac{N_H}{2.1 \times 10^{21}\ \mathrm{cm}^{-2}}\right), \quad (3)$$

where N_H is the hydrogen column density and the mean gas metallicity exponent s is equal to 1.6 (valid for $\lambda > 200$ nm; see Guiderdoni & Rocca-Volmerage for details).

To estimate the spatial dependence of τ_V for our simulated galaxies, we project their gas content on to a plane (say xy) with the aim of averaging the cold gas distribution as a function of projected distance to the centre. Using the obtained $\tau_V(r)$ radial profile, we compute the differential dust-attenuated luminosity contributed by every star particle in a given point (x, y) using its z-position as a proxy of its obscuration level, i.e. proportional to the amount of intervening cold gas between them and the galaxy outskirts. As a consequence, star particles behind the parent galaxy receive the total attenuation corresponding to its radial position $\tau_V(r)$, while those ahead are almost not attenuated at all. The luminosity of stellar populations with intermediate z-positions is accordingly affected.

As an example, in the top panel of Fig. 2 we show the visible optical depth averaged over projected radial bins in one of the most massive galaxies present in the simulation. As stated above, this quantity depends on both the metallicity and the column density of cold gas present in the system; hence, the visible optical depth tends to be higher in the inner regions of our hydrodynamical galaxies. This is due to the fact that, in the simulation, the galactic central regions tend to have higher column densities with highly enriched gas. In the bottom panel, we plot the fraction of luminosity attenuation for star particles in both b_j and K bands as a function of central distance (open and filled circles, respectively). As expected, it can be seen that the attenuation correlates with the optical depth profile and that it is stronger for bluer bands.

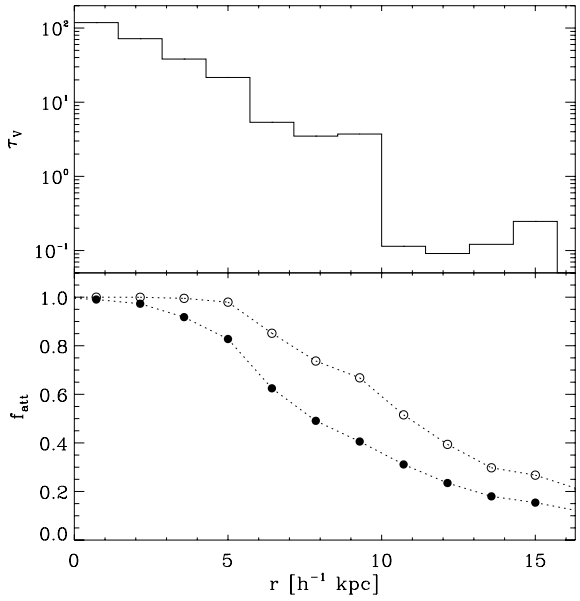

Figure 2. Estimated optical depth profile in the V band for one of the most massive BCGs in the simulation including extended intra-cluster light ($M_* \sim 10^{13}\,M_\odot$) averaged over radial projected bins (top panel) and its correspondingly smoothed attenuation fraction due to dust (bottom panel) for the b_j and K bands (open and filled circles, respectively).

Finally, we integrate over all stellar populations in order to estimate a global corrected magnitude for each galaxy in the volume (see equation 1). In the rest of the paper, we will always use *dust-attenuated* quantities unless explicitly stated.

3 RESULTS

3.1 Luminosity functions

In Fig. 3, we plot the K- and b_j-band LFs both for the simulated galaxies at $z = 0$ and for the observed local ones determined by Cole et al. (2001), Huang et al. (2003) and Norberg et al. (2002), respectively. In order to match observations at $M_* - 5\log h$, we renormalized our model LFs in each case. In relation to this, we note that the number density of L_* galaxies in our simulation gives a value roughly two times smaller than what is observed in each band. This fact is also consistent with the number density we obtain for simulated galaxies having a typical stellar mass value when comparing with the local stellar mass function (e.g. Li & White 2009). This can be due to several reasons. First, the background cosmology gives a baryon fraction which is smaller than what latest observations suggest. Secondly, the underlying numerical resolution adopted here (due to the large volume captured) can affect the assembly of small mass systems, thus preventing them from being the building blocks of more massive galaxies. These two facts combined could give rise to less galaxies of a given stellar mass. However, it is interesting to note that this is in line with the findings by Saro et al. (2006), where a similar deficit for galaxies within clusters was found, i.e. galaxy number above a given magnitude threshold tends to be smaller than observations by a factor of a few.

To show the effect of our dust implementation, we plot both the attenuated (dashed line) and non-attenuated (solid line) LFs. As expected, dust extinction is more important in the b_j band mainly affecting in this case the brightest (and gas-rich) systems. As can be seen in this figure, the simulations are not able to reproduce the bright end of the LFs given by the observations. This is due to gas cooling excess on to the dark matter potential wells that leads to an overproduction of stars in the most massive objects. As mentioned in Section 1, this behaviour was first pointed out by SAMs indicating the need for a mechanism capable of suppressing SF as a function of time and halo mass. Nowadays, there is a growing body of evidence, from both theory and observations, that AGN feedback can play an important role in this respect (e.g. Bower et al. 2006; Croton et al. 2006; Rafferty et al. 2006; Malbon et al. 2007; Khalatyan et al. 2008; Lagos et al. 2008; Cattaneo et al. 2009), although the subject is far from being completely understood.

In the same spirit as early SAMs (see below), we approximate the SF suppression in massive haloes ignoring a given fraction of the formed stars, using the stellar population ages and the maximum circular velocities of the parent galaxies present in the $z = 0$-selected subhaloes of SUBFIND as a proxy. The maximum circular velocities serve as a measure of subhalo mass and, hence, they can be used to estimate the virial velocity of the systems. The relation between the maximum circular velocity and the virial velocity for haloes in the simulation can be seen in Fig. 4. For each resolved galaxy, we apply a selective cut-off to the stellar populations that were born at different epochs to mimic the required SF suppression and test for its effect on the LFs and other observables. For the sake of simplicity, we assume a linear relationship between the subhalo

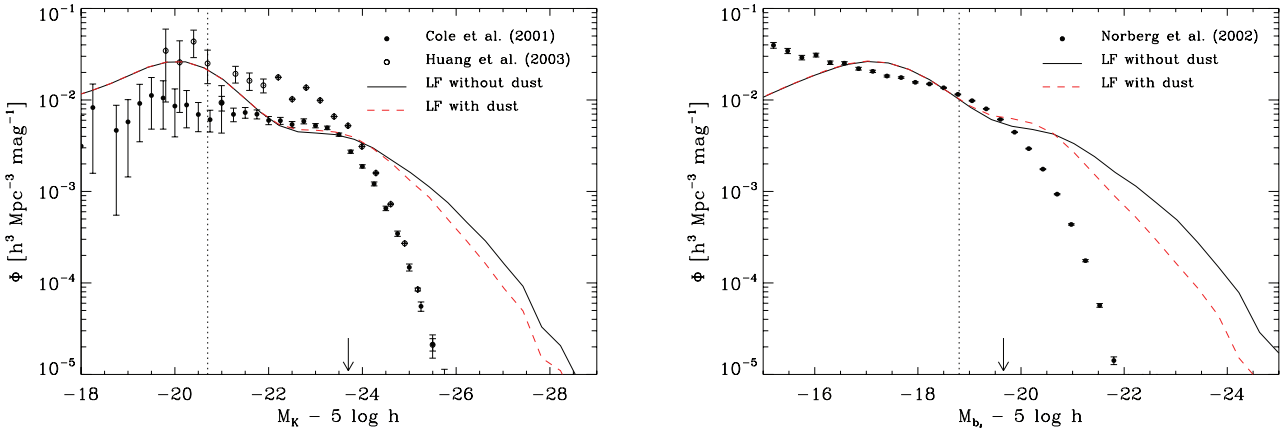

Figure 3. LFs for the simulated hydrodynamical galaxies at $z = 0$ in comparison with the observations of Cole et al. (2001) and Huang et al. (2003) for the K band (left-hand panel) and Norberg et al. (2002) for the b_j band (right-hand panel). The simulated LFs are renormalized to match observations at $M_* - 5 \log h$ (indicated by an arrow; see the text). The dashed and solid lines show the resulting LFs for the dust-attenuated and non-attenuated cases, respectively. The approximate resolution limit of the simulation in each band is indicated by the vertical dotted lines.

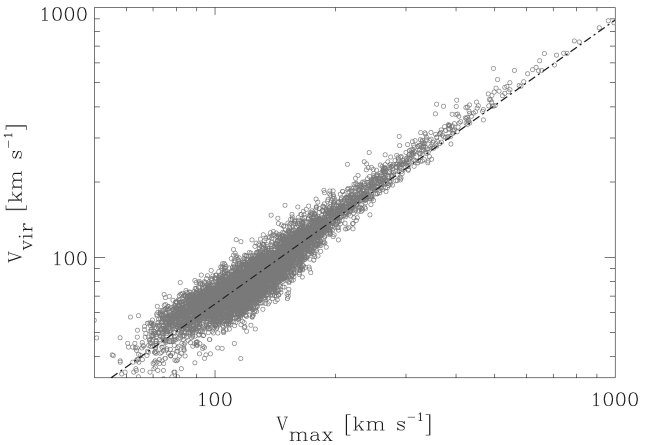

Figure 4. Halo virial velocity as a function of halo maximum circular velocity in the simulation. The dot–dashed line corresponds to the best linear fit.

Table 1. Simple SF suppression recipe: $z_{\rm cut} = (V_{\rm max} - V_0)/V_1$, where $z_{\rm cut}$ represents the redshift since which we do not consider SF in a given galaxy. Systems having $V_{\rm max} < V_0$ are not affected by the suppression.

Model	V_0 (km s^{-1})	V_1 (km s^{-1})
1	100	150
2	100	200
3	100	250
4	150	150
5	150	200
6	150	250
7	200	150
8	200	200
9	200	250

maximum circular velocity $V_{\rm max}$ and the redshift from which we do not take into account the newly formed stars $z_{\rm cut}$, as follows:

$$V_{\rm max} = V_0 + z_{\rm cut} V_1, \quad (4)$$

where V_0 and V_1 are free parameters. Although it is a very simplified parametrization aiming at *reconciling* the bright end's LF problem, it should allow us to explore the behaviour of SF suppression in a simple way. Given a (V_0, V_1) pair, the net result of this recipe is to only affect systems above the velocity limit given by the zero-point of the relation V_0, regulating the *strength* of the suppression with its slope V_1. The different models explored for this suppression scheme can be seen in Table 1.

This procedure is similar to what was done in earlier semi-analytic work, where switching off gas cooling in haloes over a certain mass threshold was a common procedure to avoid excessive SF (e.g. Kauffmann et al. 1999; Hatton et al. 2003; Cattaneo et al. 2006; Cora 2006). Nevertheless, it is fair to note that in our simple scheme, it is not possible to ignore the non-trivial interaction between the non-selected stars in a given halo and the surrounding medium for $z < z_{\rm cut}$, which will mainly affect the column density estimates for the suppressed systems. For instance, the effect of SN feedback due to the ignored stars is able to heat up the surrounding gas lowering the cold gas fraction. In the same way, the presence of these stars in the simulation will also pollute the gas phase with more chemical elements, accordingly affecting the dust properties of the medium. However, within the simple suppression framework adopted here, a more detailed model for dust extinction taking into account these facts is beyond the scope of this paper.

We show the outcome of applying this scheme in Figs 5 and 6 for different parameter choices, where the K- and b_j-band LFs can be seen. In the left-hand panels, three different models are shown maintaining V_1 fixed at 200 km s^{-1}, whereas V_0 adopt the values 100, 150 and 200 km s^{-1} (models 2, 5 and 8 of Table 1; long-dashed, dotted and solid lines, respectively). As can be seen, varying the zero-point of the relation produces a horizontal shift in the resulting LF keeping its shape almost unchanged. Reducing V_0 increases the number of suppressed galaxies, thus limiting the number of systems at a given luminosity. In the right-hand panels, we also show three different models but fixing V_0 at 200 km s^{-1} and letting V_1 adopt the values 150, 200 and 250 km s^{-1} (models 7, 8 and 9 of Table 1; three-dot–dashed, solid and dot–dashed lines, respectively). In this case, all model LFs coincide at $\sim M_* - 5 \log h$ showing appreciable differences only in the bright end. This reflects the strength of SF suppression recipe in more massive haloes.

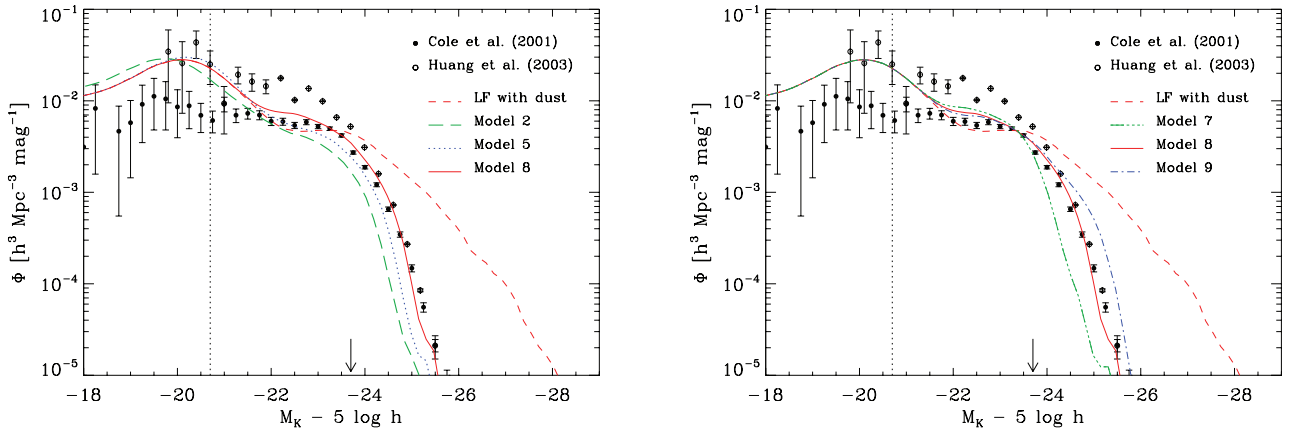

Figure 5. *K*-band field LF at $z = 0$ for different SF suppression models (left-hand panel: long-dashed, dotted and solid lines which correspond to models 2, 5 and 8 of Table 1, respectively; right-hand panel: three-dot–dashed, solid and dot–dashed lines which correspond to models 7, 8 and 9 of Table 1, respectively). The solid lines in both panels correspond to the *best-fitting* model. The simulated LFs are renormalized to match observations at $M_* - 5\log h$ (indicated by an arrow; see the text). As a comparison, we plot as a dashed line the dust-attenuated LF without SF suppression. The approximate resolution limit of the simulation in each band is indicated by the vertical dotted line.

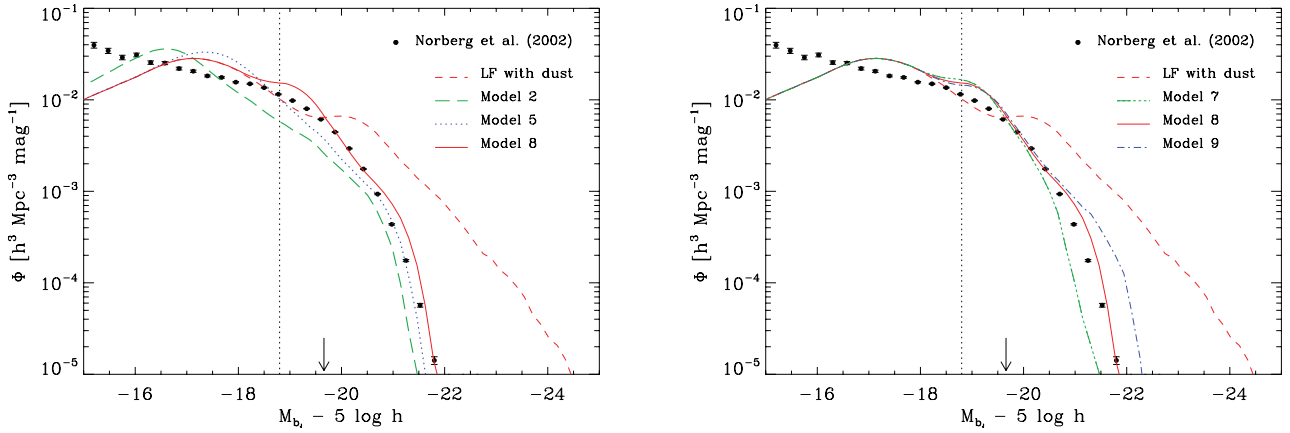

Figure 6. Same as Fig. 5, but for the $b_{\rm j}$-band field LF.

For the explored models, the best agreement with observations is obtained for $(V_0, V_1) = (200, 200)\,{\rm km\,s^{-1}}$ (model 8; see Table 1). This maximum circular velocity value roughly corresponds to $V_{\rm vir} \sim 150\,{\rm km\,s^{-1}}$, as can be seen from Fig. 4. In this model, systems with $V_{\rm vir} \lesssim 150\,{\rm km\,s^{-1}}$ are not affected by the SF quenching and those having $V_{\rm vir} \gtrsim 300\,{\rm km\,s^{-1}}$ are suppressed since $z \gtrsim 1$, in agreement with previous SAM findings which take into account physically motivated AGN feedback models (e.g. Croton et al. 2006). In what follows, we will refer to this case as the *best-fitting* model. Even though in this case there is a much better agreement with data in the bright end compared to the non-suppression case, some improvement is still needed in the faint end with the simulation results typically overpredicting the number density of galaxies per magnitude bin in relation to observations. As mentioned in Section 1, it is believed that stellar feedback should be more efficient in smaller galaxies. Nevertheless, higher resolution simulations are needed in order to study this effect.

Given the size of the simulated volume, it is possible to study the distribution of luminosities in the groups and galaxy clusters formed. However, we do not pretend here to make a rigorous comparison with observations since we will address this issue in future work using high-resolution runs. Instead, we just select all galaxies belonging to groups with virial mass higher than $10^{13}\,h^{-1}\,{\rm M}_\odot$ as our galaxy sample. In Fig. 7, we show the luminosity distribution of this sample for the SDSS *r* and *z* bands together with the fit to the data given by Popesso et al. (2006) for the RASS-SDSS galaxy cluster survey (smooth solid line). To take into account the (arbitrary) adopted normalization in observations, our cluster LFs are forced to match the data at $M_{r,z} = -20$. As can be seen, the *best-fitting* model (solid line) does a better work in describing the observed profiles than the dust-attenuated only luminosity distribution (dashed line). This is also true if we study the BCG luminosity as a function of halo mass. Fig. 8 shows the *K*-band luminosity–halo mass relation for BCGs residing in haloes with $M_{\rm vir} > 10^{13}\,h^{-1}\,{\rm M}_\odot$ in both mentioned cases (open and filled circles, respectively), compared to the observational trend given by Brough et al. (2008) (dot–dashed line). It can be seen that the suppression scenario displays a better agreement with data, although the suppression seems to be somewhat stronger than needed for the most massive systems.

3.2 Galaxy colours

In Fig. 9, we show the distribution of galaxies in our simulated local volume projected on to the sky. The galaxies are colour coded using their $B - V$ colours in the *best-fitting* suppression case. From this figure it can be stated qualitatively that redder hydrodynamical

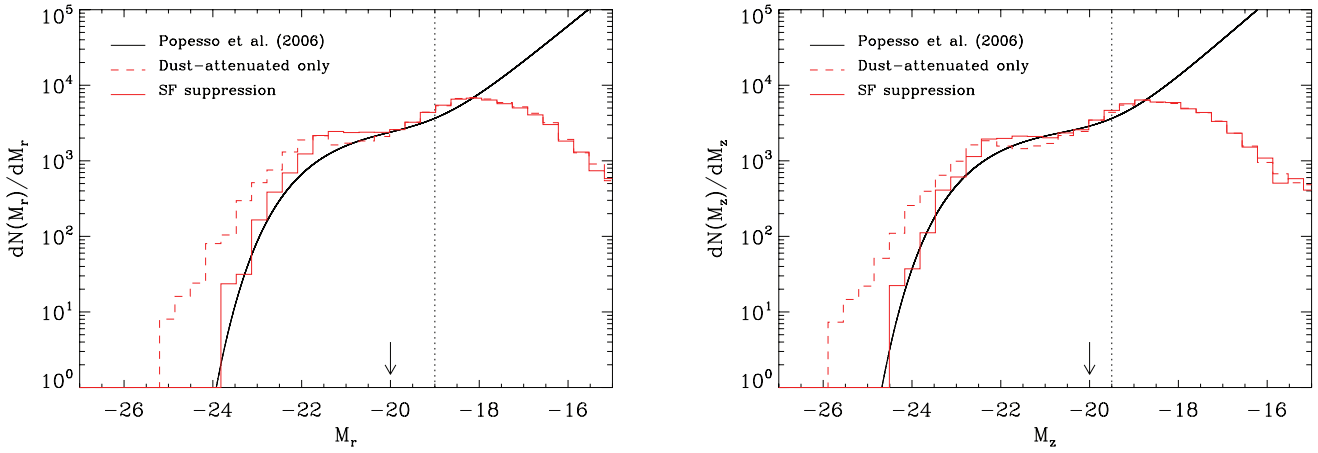

Figure 7. Luminosity distribution for galaxies in groups and clusters for the SDSS r band (left-hand panel) and z band (right-hand panel) in the simulation. The best fit to data in the RASS-SDSS galaxy cluster survey given by Popesso et al. (2006) is also shown as a smooth solid line. The dashed lines correspond to simulated cluster galaxies without SF quenching in massive haloes, while the solid ones correspond to the *best-fitting* SF suppression case. The simulated result is forced to match observations at $M_{r,z} = -20$ (indicated by an arrow; see the text). The approximate resolution limit of the simulation in each band is indicated by the vertical dotted lines.

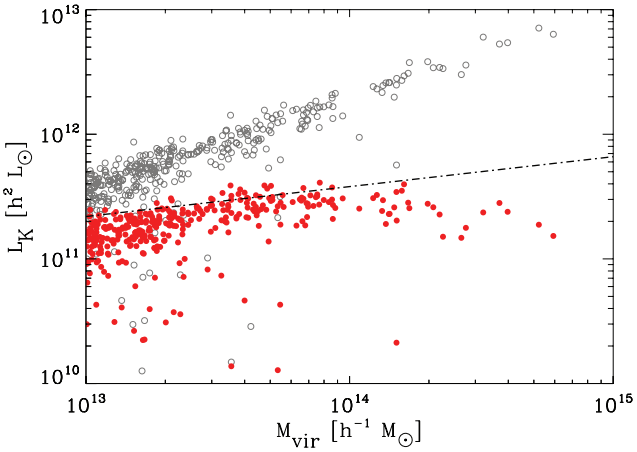

Figure 8. Luminosity–halo mass relation for BCGs in the simulation showing the K-band luminosity as a function of their virial mass in comparison with the observational trend (dot–dashed line) given by Brough et al. (2008). Open circles stand for the SF non-suppression case, while filled ones represent our *best-fitting* SF quenching scenario.

galaxies tend to inhabit high density environments, in contrast to galaxies populating the field, generally bluer. A similar trend is obtained for the plain simulation output, although in that case there is an excess of blue systems in cluster environments.

The effect of SF suppression in the colours of galaxies is easily seen in Fig. 10. In this figure, we show the $B - V$ colour index of numerically resolved galaxies against their stellar masses for the non-suppression case (filled circles) and what results for the *best-fitting* suppression procedure presented above (contour lines). Interestingly, the hydrodynamical galaxy population of the non-suppressed simulation shows a clear colour bimodality for a given stellar mass, where two main branches can be easily seen. Those systems with the colour index satisfying $B - V \gtrsim 0.8$ populate the so-called *red sequence*, while the rest populate what we call the *blue cloud*. This last branch contains a blue galaxy population with $M_* \gtrsim 2 \times 10^{11}\, h^{-1}\, \mathrm{M}_\odot$ responsible for the mismatch in the bright end of the LFs shown in Fig. 3. In particular, most of the systems having $V_{\rm vir} \gtrsim 300\,\mathrm{km\,s^{-1}}$ (arrow in the right) correspond to overluminous BCGs which have acquired around 50 per cent of their stellar mass at late epochs due to the overcooling effect.

This is at variance with the SF suppression scenario (contour lines) in which most of the massive blue galaxies became redder as a result of their older stellar populations. It can be seen that many of the systems with $V_{\rm vir} \gtrsim 150\,\mathrm{km\,s^{-1}}$ (arrow in the left) have been suppressed in such a way that their colours turn redder than what observations suggest. Henceforth, it is clear from the contours that the simple procedure adopted to suppress SF is too efficient for some galaxies while not efficient enough for the most massive ones. This results in a distribution that cannot fully account for the galaxy colour bimodality in the stellar mass range $M_* \sim 2 \times 10^{10}$–$2 \times 10^{11}\, h^{-1}\, \mathrm{M}_\odot$ (e.g. Baldry et al. 2006), reflecting the fact that physically motivated feedback schemes must be considered for massive haloes in future work.

As a final remark, it is worth noting that a moderately massive red population having $M_* \sim 5 \times 10^9\, h^{-1}\, \mathrm{M}_\odot$ naturally appears in the simulation. The diamond in Fig. 10 indicates the approximate position of this population in the diagram. These systems correspond to galaxies that have assembled most of their stellar mass at early epochs, being satellites whose gas content have been stripped off when accreted by central objects. This mechanism removes gas from galaxies limiting new SF and, as a consequence, stellar populations become older and redder.

3.3 Clustering properties

In this section, we explore the clustering properties of galaxies in the simulation, both for the non-suppressed and for the *best-fitting* SF suppression cases. The left-hand panel of Fig. 11 shows the real-space two-point correlation function for galaxies in the plain simulation with different $b_{\rm j}$-band absolute magnitudes (filled symbols). Circles are related to galaxies with $-20 < M_{b_{\rm j}} - 5\log h < -19$, while squares and diamonds show the resulting correlations for all galaxies brighter than -20 and -21, respectively. We also plot as dashed and three-dot–dashed lines the observational trends found by Norberg et al. (2001) for $\sim L_*$ and $\sim 4L_*$ galaxies (corresponding to $M_{b_{\rm j}} - 5\log h \simeq -19.5$ and -21.5, respectively). In the first place, it can be seen that brighter galaxies cluster strongly than fainter ones, as expected. The agreement with observations is fairly good taking

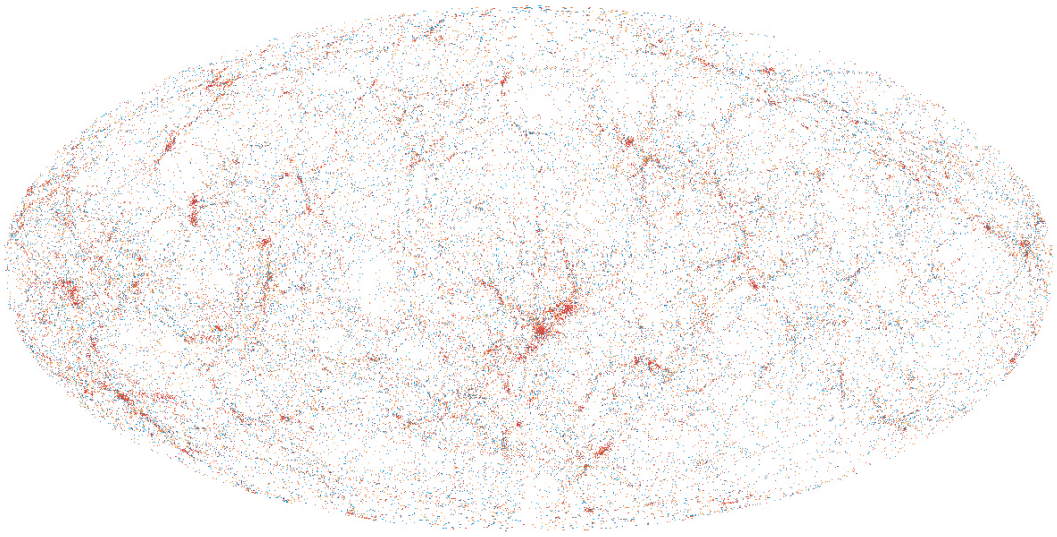

Figure 9. Same as Fig. 1, but for the galaxy distribution colour-coded from blue to red by their $B-V$ colours ($0.3 < B-V < 1$) in the *best-fitting* SF suppression case. Hydrodynamical galaxies with redder colours tend to inhabit high density regions in contrast to bluer systems populating the field.

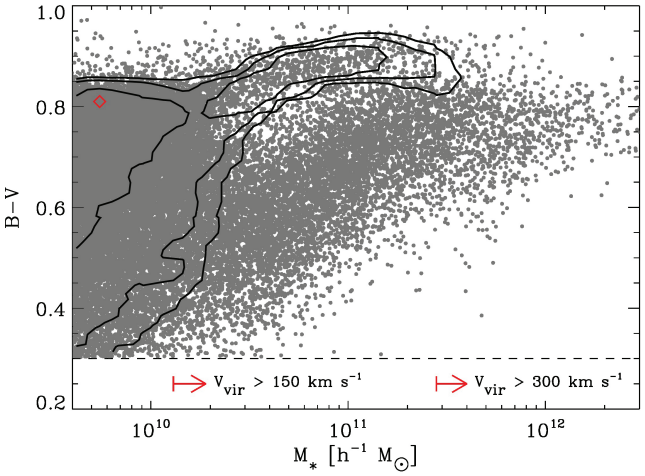

Figure 10. $B-V$ galaxy colours as a function of their stellar mass for the numerically resolved galaxy population at $z=0$. Filled circles stand for the case without SF quenching, while contour lines contain 55, 85 and 95 per cent of the galaxy population in the *best-fitting* SF suppression scenario. Arrows indicate lower bounds for the virial velocity of systems with a given stellar mass: $V_{\rm vir} \gtrsim 150$ and 300 km s^{-1}, respectively. The diamond indicates the approximate position of the satellite galaxy population in the diagram.

into account the fact that normalization is a natural outcome of the simulation. In particular, for $\sim L_*$ galaxies (circles) the clustering pattern shows a power-law behaviour similar to that observed, although the agreement is worse for higher scales ($\gtrsim 10\,h^{-1}$ Mpc). Likewise, for systems with $M_{b_{\rm j}} - 5\log h < -21$ (diamonds) the agreement with observations is encouraging.

It is also interesting to investigate the clustering of galaxies as a function of their SF activity parametrized using galaxy colours. At $z \sim 0$, passive systems tend to populate high density environments, having redder colours, in contrast to active systems which are mainly located in the field (e.g. Balogh et al. 2004; Baldry et al. 2004, 2006). We define as *passive* systems all galaxies having $B-V > 0.8$, while *active* systems satisfy $B-V < 0.8$. The right-hand panel of Fig. 11 shows the real-space two-point correlation function for passive red galaxies (diamonds) and bluer ones (circles) in comparison with the observed correlations (valid for scales between $\sim$0.1 and 20 h^{-1} Mpc) given by Madgwick et al. (2003). It is easy to see that both populations are clearly separated, with redder systems clustering more strongly and displaying a similar behaviour to observations. For passive systems, there is a substantial excess of power and a clear departure from a power law. The power excess in this case is due to the fact that the overcooling present in the simulation decreases the number density of red systems, thus increasing the value of the correlation length.

On the other hand, Fig. 12 shows the outcomes when considering the *best-fitting* suppression scheme. From its left-hand panel, it can be seen that the correlation function for $\sim L_*$ galaxies (circles) exhibits essentially the same behaviour as before (compare with Fig. 11) while displaying appreciable differences only for brighter galaxies (squares and diamonds). For objects brighter than $M_{b_{\rm j}} - 5\log h = -21$, the result is affected by low number statistics leading to a noisier correlation function that is somewhat off from the observational expectation. This is partially overcome when including more galaxies in the $M_{b_{\rm j}} - 5\log h > -20$ case. Active galaxies present an excellent agreement with data for all studied scales (right-hand panel of Fig. 12), and the discrepancy with observations found for passive red systems found in Fig. 11 is alleviated. This is somewhat expected since, as can be seen from the contour lines of Fig. 10, after the SF quenching, many of the galaxies have migrated to the *red sequence* increasing the number density of passive systems. Despite this improvement, it is important to remember that the colour–stellar mass relation is not well reproduced in this case due to the simplistic approach adopted to *redden* galaxies more massive than $V_{\rm vir} \gtrsim 150$ km s^{-1}.

4 SUMMARY AND CONCLUSIONS

In this paper, we have focused on the luminosity, colour and clustering properties of galaxies that arise naturally in a hydrodynamical cosmological simulation of structure formation. The spherical local volume of $\sim 130^3\,h^{-3}$ Mpc^3 was simulated using the *zooming* technique with more than $\sim$50 million gas and dark matter particles. In particular, our simulation code includes different physical

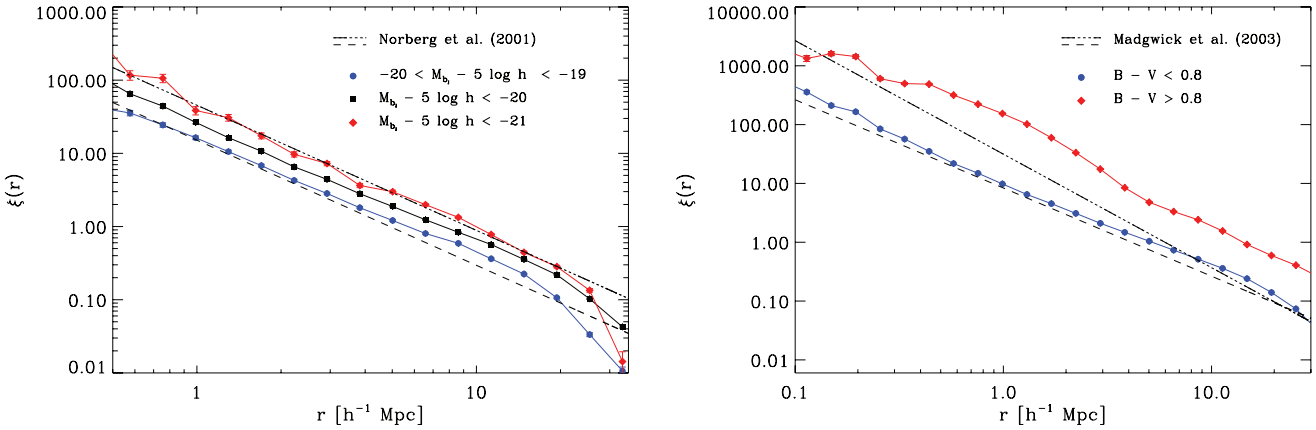

Figure 11. Real space two-point correlation function for the simulated galaxies without SF quenching (filled symbols) in different b_j-band magnitude bins (left-hand panel) and colour populations (right-hand panel). The error bars denote Poissonian fluctuations. Observational trends from Norberg et al. (2001) for $\sim L_*$ and $\sim 4L_*$ galaxies, and from Madgwick et al. (2003) for *active* and *passive* galaxies are shown as dashed and three-dot–dashed lines, respectively. The observations are valid in the range ~ 0.1–$20\,h^{-1}$ Mpc.

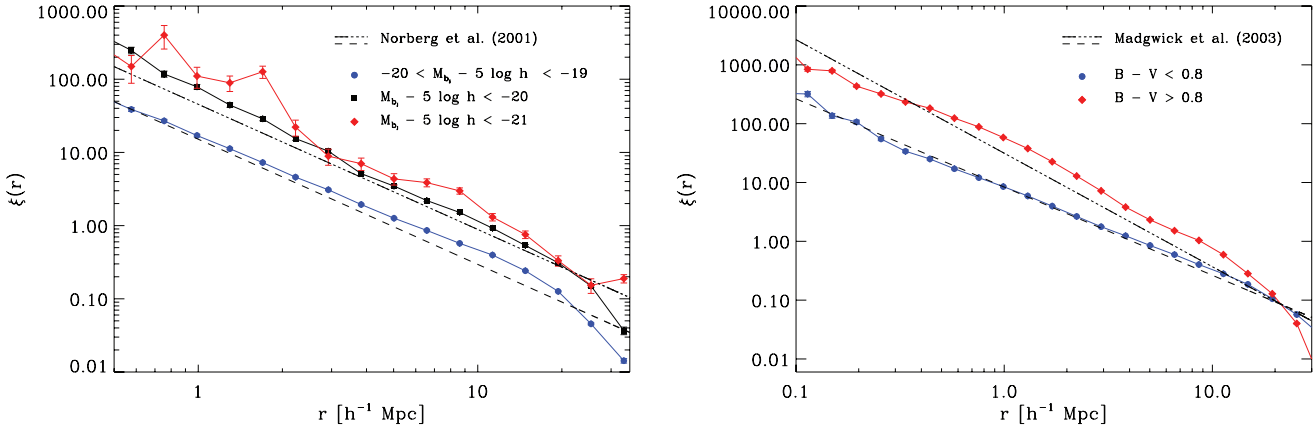

Figure 12. Same as Fig. 11, but for galaxies in the *best-fitting* post-processing scheme to suppress SF.

mechanisms such as SN feedback, galactic winds, a UV pervading background since $z \sim 6$ and chemical enrichment of the gas and stellar populations as time elapses. However, we have not explicitly included a physical mechanism capable of quenching SF in massive haloes (such as AGNs). In this way, by $z = 0$ a total of $\sim$20 000 objects having more than 32 star particles are formed in the volume. The luminosities of the hydrodynamical galaxies were computed using the differential contribution provided by every star particle present inside the optical radius of the systems. As a way of estimating the dust-attenuated luminosity in the bands of interest, we implemented a simple model for dust extinction that makes use of the cold gas distribution in each galaxy as a tracer of its dust content. In order to mimic the required SF suppression in massive (i.e. $V_{\rm vir} \gtrsim 150\,{\rm km\,s^{-1}}$) haloes, we also applied a simple recipe to the present-day output of the simulation to reconcile the bright end of the simulated LFs with observations and to further investigate its inclusion in other properties of the simulated galaxies. In the following, we summarize the main conclusions of this work.

(i) As shown earlier by semi-analytic work, it is essential to suppress SF in massive haloes to describe the bright end of the field LF at $z \sim 0$. For instance, haloes with masses corresponding to $V_{\rm vir} \sim 300\,{\rm km\,s^{-1}}$ are required to quench their SF since $z \sim 1$ in the *best-fitting* SF suppression case. In this way, it is possible to avoid the formation of very bright blue BCGs in the simulation. However, after a small renormalization to L_*, the faint end of the simulated field LFs tends to overpredict the number density of galaxies per magnitude bin in the b_j band for galaxies with luminosities lower than $\sim L_*$. To better study this effect, higher resolution simulations are needed.

(ii) The group/cluster bright-end luminosity distributions are better described when SF suppression is considered. This is due to the fact that massive cluster satellites used to be BCGs in the past and also require some level of SF suppression. However, as a consequence of our relatively high-mass galaxy resolution limit we cannot confirm the upturn of faint cluster satellites in the cluster LF function as previously obtained by Saro et al. (2006, 2009) using high-resolution resimulations of galaxy clusters. On the other hand, the K-band luminosity–halo mass relation that naturally arises in the simulation also needs further SF quenching in massive haloes to better describe observations given by Brough et al. (2008).

(iii) The stellar masses of the hydrodynamical galaxies in the plain simulation display a clear $B - V$ colour bimodal behaviour as suggested by observations (e.g. Baldry et al. 2006), although the *active* blue galaxies present very massive systems, due to overcooling, contrary to what data show. When taking into account the SF suppression scheme, the $B - V$ galaxy colours turn redder, displaying a colour–stellar mass distribution that is not able to fully account

for observations. In this case, a bimodal distribution is observed for stellar masses lower than $\sim 2 \times 10^{10}\, h^{-1}\, \mathrm{M}_{\odot}$, while for higher masses most of the galaxies are red. This is a manifestation of the rough nature of the simple parametrization adopted to quench SF in massive haloes.

(iv) The clustering properties of different hydrodynamical galaxy populations that naturally arise in the simulation are in qualitative agreement with observational results. The scale-dependent correlation function of our $\sim L_*$ objects in the b_j band displays a power-law behaviour up to $\sim 10\, h^{-1}$ Mpc that is in good agreement with data given by Norberg et al. (2001). As expected, higher luminosity systems show a stronger clustering pattern, where galaxies having luminosities around $\sim 4L_*$ display an excellent agreement with observations. On the other hand, it is also possible to disentangle the galaxy correlation properties when the sample is split by galaxy colours. The correlation function of *active* blue ($B - V < 0.8$) systems is in rough agreement with the results given by Madgwick et al. (2003). However, *passive* red systems ($B - V > 0.8$) present an excess of power in comparison with observations, showing a clear departure from the power-law behaviour. As shown when using the SF suppression scheme, this discrepancy is alleviated when more galaxies are able to populate the *red sequence* of the colour–magnitude diagram. This is due to the fact that, typically, the added systems tend to reside in less clustered haloes, thus lowering the correlation length value.

In summary, we conclude that analysing the global properties of the galaxy population within hydrodynamical, cosmological simulations starts to be a promising tool to study galaxy evolution. Current simulations already fairly represent the underlying hydrodynamical effects (at least in a global sense) and, in general, describe the SF process well enough to qualitatively reproduce observed environmental trends. However, similar to the widely used SAMs, overcooling in massive haloes has to be quenched by additional feedback effects. It has to be seen in future simulations, which directly include such additional processes, if such a quenching happens mildly enough not to destroy some of the general trends already captured in the current generation of hydrodynamical simulations.

ACKNOWLEDGMENTS

The authors would like to thank the referee, Adrian Jenkins, for several comments that helped to improve this paper. SEN acknowledges G. De Lucia, E. Puchwein, A.G. Sánchez, F. Stasyszyn and C. Scannapieco for useful discussions and Deutscher Akademischer Austausch Dienst (DAAD) for support. KD acknowledges support by the DFG Priority Programme 1177.

REFERENCES

Baldry I. K., Glazebrook K., Brinkmann J., Ivezić Z., Lupton R. H., Nichol R. C., Szalay A. S., 2004, ApJ, 600, 681
Baldry I. K., Balogh M. L., Bower R. G., Glazebrook K., Nichol R. C., Bamford S. P., Budavari T., 2006, MNRAS, 373, 469
Balogh M. L., Baldry I. K., Nichol R., Miller C., Bower R., Glazebrook K., 2004, ApJ, 615, 101
Baugh C. M., Gaztañaga E., Efstathiou G., 1995, MNRAS, 274, 1049
Blanton M. R. et al., 2001, AJ, 121, 2358
Blanton M. R. et al., 2003, ApJ, 592, 819
Bower R. G., Benson A. J., Malbon R., Helly J. C., Frenk C. S., Baugh C. M., Cole S., Lacey C. G., 2006, MNRAS, 370, 645
Brough S., Couch W. J., Collins C. A., Jarrett T., Burke D. J., Mann R. G., 2008, MNRAS, 385, 103
Bruzual G., Charlot S., 2003, MNRAS, 344, 1000
Cattaneo A., Dekel A., Devriendt J., Guiderdoni B., Blaizot J., 2006, MNRAS, 370, 1651
Cattaneo A. et al., 2009, Nat, 460, 213
Charlot S., Fall S. M., 2000, ApJ, 539, 718
Cole S. et al., 2001, MNRAS, 326, 255
Crain R. A. et al., 2009, MNRAS, 399, 1773
Croton D. J. et al., 2006, MNRAS, 365, 11
Colless M., 1999, R. Soc. London Philos. Trans. A, 357, 105
Colless M. et al., 2001, MNRAS, 328, 1039
Cora S., 2006, MNRAS, 368, 1540
Davé R., Oppenheimer B. D., 2007, MNRAS, 374, 427
De Lucia G., Blaizot J., 2007, MNRAS, 375, 2
De Lucia G., Kauffmann G., White S. D. M., 2004, MNRAS, 349, 1101
Dolag K., Hansen F. K., Roncarelli M., Moscardini L., 2005, MNRAS, 363, 29
Dolag K., Borgani S., Murante G., Springel V., 2009, MNRAS, 399, 497
Fisher K. B., Davis M., Strauss M. A., Yahil A., Huchra J., 1994, MNRAS, 266, 50
Fisher K. B., Huchra J. P., Strauss M. A., Davis M., Yahil A., Schlegel D., 1995, ApJS, 100, 69
Fontanot F., De Lucia G., Monaco P., Somerville R. S., Santini P., 2009, MNRAS, 397, 1776
Guiderdoni B., Rocca-Volmerange B., 1987, A&A, 186, 1
Guo Q., White S. D. M., 2009, MNRAS, 396, 39
Haardt F., Madau P., 1996, ApJ, 461, 20
Hatton S., Devriendt J. E. G., Ninin S., Bouchet F. R., Guiderdoni B., Vibert D., 2003, MNRAS, 343, 75
Hawkins E. et al., 2003, MNRAS, 346, 78
Hoffman Y., Ribak E., 1991, ApJ, 380, 5
Huang J. S., Glazebrook K., Cowie L. L., Tinney C., 2003, ApJ, 584, 203
Kauffmann G., Colberg J. M., Diaferio A., White S. D. M., 1999, MNRAS, 303, 188
Khalatyan A., Cattaneo A., Schramm M., Gottlöber S., Steinmetz M., Wisotzki L., 2008, MNRAS, 387, 13
Kolatt T., Dekel A., Ganon G., Willick J. A., 1996, ApJ, 458, 419
Lagos C. D. P., Cora S. A., Padilla N. D., 2008, MNRAS, 388, 587
Li C., White S. D. M., 2009, MNRAS, 398, 2177L
Lin H., Kirshner R. P., Shectman S. A., Landy S. D., Oemler A., Tucker D. L., Schechter P. L., 1996, ApJ, 464, 60
Madgwick D. S. et al., 2003, MNRAS, 344, 847
Maeder A., Meynet G., 1989, A&A, 210, 155
Malbon R. K., Baugh C. M., Frenk C. S., Lacey C. G., 2007, MNRAS, 382, 1394
Mathis H., Lemson G., Springel V., Kauffmann G., White S. D. M., Eldar A., Dekel A., 2002, 333, 739
Matteucci F., Recchi S., 2001, ApJ, 558, 351
Norberg P. et al., 2001, MNRAS, 328, 64
Norberg P. et al., 2002, MNRAS, 336, 907
Nuza S. E., Tissera P. B., Pellizza L. J., Lambas D. G., Scannapieco C., de Rossi M. E., 2007, MNRAS, 375, 665
Ocvirk P., Pichon C., Teyssier R., 2008, MNRAS, 390, 1326
Oppenheimer B. D., Davé R., 2006, MNRAS, 373, 1265
Oppenheimer B. D., Davé R., 2008, MNRAS, 387, 577
Pearce F. R., Jenkins A., Frenk C. S., White S. D. M., Thomas P. A., Couchman H. M. P., Peacock J. A., Efstathiou G., 2001, MNRAS, 326, 649
Popesso P., Böhringer H., Brinkmann J., Voges W., York D. G., 2004, A&A, 423, 449
Popesso P., Biviano A., Böhringer H., Romaniello M., 2006, A&A, 445, 29
Rafferty D. A., McNamara B. R., Nulsen P. E. J., Wise M. W., 2006, ApJ, 652, 216
Recchi S., Matteucci F., D'Ercole A., 2001, MNRAS, 322, 800
Salpeter E. E., 1955, ApJ, 121, 161
Saro A., Borgani S., Tornatore L., Dolag K., Murante G., Biviano A., Calura F., Charlot S., 2006, MNRAS, 373, 397
Saro A., De Lucia G., Dolag K., Borgani S., 2008, MNRAS, 391, 565

Saro A., Borgani S., Tornatore L., De Lucia G., Dolag K., Murante G., 2009, MNRAS, 392, 795
Spergel D. N. et al., 2003, ApJS, 148, 175
Springel V., 2005, MNRAS, 364, 1105
Springel V., Hernquist L., 2002, MNRAS, 333, 649
Springel V., Hernquist L., 2003, MNRAS, 339, 289
Springel V., White S. D. M., Tormen G., Kauffmann G., 2001, MNRAS, 328, 726
Springel V. et al., 2005, Nat, 435, 629
Sutherland R. S., Dopita M. A., 1993, ApJS, 88, 253
Tornatore L., Borgani S., Matteucci F., Recchi S., Tozzi P., 2004, MNRAS, 349, 19
Tornatore L., Borgani S., Dolag K., Matteucci F., 2007, MNRAS, 382, 1050
White M., Hernquist L., Springel V., 2001, preprint (astro-ph/0107023)
York D. G. et al., 2000, AJ, 120, 1579
Yoshikawa K., Taruya A., Jing Y. P., Suto Y., 2001, ApJ, 558, 520
Zehavi I. et al., 2002, ApJ, 571, 172

This paper has been typeset from a TEX/LATEX file prepared by the author.